Composites of Plasma Surface Functionalized Barium Titanate Nanoparticles Covalently Attached to Epoxide Matrices: Synthesis and Evaluation

Narayan Mukherjee, Dattatray Wavhal, and Richard B. Timmons*

Department of Chemistry and Biochemistry, University of Texas at Arlington, 700 Planetarium Place, Arlington, Texas 76019-0065

ABSTRACT Inorganic/organic nanocomposites consisting of surface functionalized barium titanate (BTO) nanoparticles covalently bonded to epoxy polymeric matrices are described. A plasma-enhanced CVD process was employed to functionalize the particle surfaces with reactive amine groups. Subsequently, these modified particles were reacted with an epoxide monomer to synthesize the final nanocomposites, containing particle loadings ranging from 1 to 5 weight percent. Control samples, containing unmodified BTO, were also synthesized under identical reaction conditions and particle loading. The resultant nanocomposites were characterized spectroscopically and microscopically, and their physical and thermal properties were evaluated. The results obtained reveal a more uniform distribution of the surface modified BTO in the composites relative to that observed with the unmodified particles. Additionally, the physical and thermal properties of the nanocomposites containing the plasma modified particles were determined to be significantly improved over that of the pure polymer or the composites containing the unmodified particles, for each level of loading employed in this study. In light of these improved properties, it appears that the surface modifications employed significantly improve the interfacial interactions between the inorganic particles and the organic matrices in these nanocomposites.

KEYWORDS: inorganic/organic nanocomposites • plasma functionalized particles • covalently bonded • enhanced physical properties • plasma enhanced CVD • barium titanate-epoxy composite

INTRODUCTION

One of the more active nanotechnology research areas is that dealing with synthesis of inorganic/organic nanocomposites. In part, this activity reflects the increasing availability of inorganic nanoparticles with respect to sizes, shapes, and compositions. From the practical standpoint, it has become increasingly apparent that such nanocomposites provide an opportunity for synthesis of improved polymeric materials with respect to mechanical, thermal stability, magnetic, flame inhibition, and optoelectronic properties (1).

Although significant advances have been reported with these materials, a persistent difficulty encountered among workers in this field pertains to the general inherent incompatibility between inorganic and organic compounds with respect to achieving uniform mixtures. With respect to synthesis of these composites, the mixing problems are frequently acute. This difficulty arises from the fact that the inorganic components are most frequently hydrophilic metal oxides, whereas the organic monomers are generally nonpolar and thus more hydrophobic in nature. This disparity in polarities tends to promote inorganic particle aggregation and segregation from the polymer matrix. Additionally, the mixing problem is further enhanced by the simple fact that nanoparticles have a well-documented tendency for increased aggregation as the particle sizes are decreased and surface to volume ratios increase. In light of these considerations, phase separations may occur, particularly for samples subjected to elevated temperature variations, thus limiting the potential long term usage of a particular material.

In recognition of this problem, innovative techniques have been developed to help achieve the desired particle dispersions in these inorganic/organic composites (1). Among the most prominent of these approaches is simple physical mechanical blending and sol−gel polymerization (1g, 2, 3). Although interesting results have been reported, interactions between the polymer matrix and the nanoparticles frequently exist only at discrete locations where the inorganic agglomerates are bounded with polymer, rather than uniformly dispersed throughout the polymer matrix (4). The large surface to volume ratios of the nanoparticles create relatively large interfacial regions, frequently with resultant poor adhesions between the hydrophobic organic matrix and hydrophilic inorganic filler components (5), in many cases limiting the extent of particle loading that can be realistically achieved. A particularly thorough examination of the interactions between inorganic oxide nanoparticles and polymer matrices, involving direct studies of interfacial layers between matrix and filler, and the resulting physical properties of composites are the studies of Tannenbaum et al. (4d, 5d).

* To whom correspondence should be addressed. Phone: (817) 272-3801. Fax: (817) 272-3808. E-mail: timmons@uta.edu.
Received for review October 6, 2009 and accepted January 6, 2010

DOI: 10.1021/am900677s

In view of these mixing difficulties, a number of recent studies have examined the utility of modifying the inorganic particle prior to formation of the composites with the goal of minimizing the particle dispersion problem and at the same time improving the interfacial interactions between the disparate inorganic and organic components. One such method involves initial surfactant/ligand encapsulation of the particles. Although this approach can improve the dispersion of nanoparticles in the polymer matrix, a decrease in thermal and mechanical properties, with increasing nanoparticle loading has been reported in some studies (4e). A different approach involves surface functionalization of inorganic nanoparticles, such as the use of organosilane treatment. Improved properties of the resultant composites have been reported (6) but the inherent hydrolytic instability of metal-silane linkages (metal−O−Si) is a concern with respect to long term stability considerations (7). Furthermore, availability of surface −OH groups of these inorganic nanoparticles is highly dependent on the synthetic route employed for the oxides (8). As an alternative, chemical surface grafting of some specific nanomaterials have been reported in recent years, mainly based on carbon nanotubes and montmorillonite type layered silicates (9). For example, Leu et al reported amine functionalization of layered silicates via chemical treatment of *N*,*N*-dimethylacetamide and γ-(aminopropyl)triethoxysilane (9a). Zhu et al. achieved amine functionalization of CNT via a two steps process involving initial reaction with succinic acid to form ethylcarboxyl groups on the CNT sidewall, which are then converted to amine functionalized CNTs via chemical treatment with thionyl chloride and bis(*p*-aminocyclohexyl)methane (9c). In general, nanocomposites synthesized using the functionalized particles have shown significant improvement of properties.

The present paper examines a different approach to achieving both more uniform and more stable dispersions of the inorganic particles in the organic polymeric matrices. In this work, plasma-enhanced CVD (PECVD) is employed to reduce the surface energy of the particle and, simultaneously, introduce reactive functional groups on the surfaces of the particles. In contrast with the prior work in the composites area involving particle surface modifications, the present approach is a single-step, gas-phase process. During this single step, the plasma processing parameters are continuously varied to deposit a gradient layered, conformal, strongly grafted functionalized thin organic film on the particle surfaces. These reactive functional groups, introduced during the PECVD process, are subsequently employed to covalently bind the functionalized inorganic particle to the organic monomer. This is followed by the final step involving synthesis of the inorganic/organic nanocomposite materials using conventional liquid processing reactions. Although treatment of nanoparticles via radio frequency (RF) plasmas for subsequent use in nanocomposite synthesis have been reported, the treatments have centered on attempts to improve the dispersion of the particles in the final polymeric matrices, as opposed to covalent attachment processes (10). Additionally, it should be noted that a thorough study involving plasma surface functionalization of micrometer sized polystyrene beads by Badyal et al. provided clear evidence that the extent of surface modification increases as the particle sizes were decreased (11).

In this study, we examine the properties of epoxy based nanocomposites. This selection is based on the fact that epoxies represent an important class of materials that have been examined with respect to their potential use in structural, thermal, and electronic applications in nanocomposite formulations (9c, 12). Barium titanate (BTO) is employed as the inorganic component, based on its ready availability, along with the fact that it too has frequently been employed in nanocomposite materials (12d–12f, 13). The BTO particles are initially functionalized by PECVD deposition of polymer films containing reactive amine groups. The amine groups are employed to bond the particles to an epoxide monomer, followed by polymerization and ultimate formation of the BTO/epoxy nanocomposites. The main focus of the present study was to compare and contrast the properties of the nanocomposites synthesized using the surface functionalized BTO nanoparticles with composites fabricated using the same chemistry but with unmodified BTO. As documented below, the mechanical and thermal properties of the composites exhibit significantly improved physical properties, relative to those composites containing the unmodified BTO achieved with relatively low levels of BTO loading. The properties of the composites were also observed to be significantly improved over those of the pure epoxy polymers.

EXPERIMENTAL SECTION

Materials. Ethylenediamine (EDA) was obtained from Aldrich (Milwaukee, Wisconsin) and was of the highest purity available. Bisphenol F Diglycidyl ether (Epoxy; Epon Resin 862) and triethylene tetramine (Epikure 3234) were supplied by Hexion Specialty Chemicals. Tetragonal barium titanate (BTO) nanoparticles (99.6% purity, with average particle size 85-28 nm) were purchased from Nanostructured & Amorphous Materials Inc. $BaTiO_3$ was dried in an oven at 120 °C under a vacuum prior to use. All other chemicals were used as received.

Instrumentation. X-ray photoelectron spectroscopy (XPS) was conducted utilizing a Perkin-Elmer model PHI 5000 instrument, using Al Kα radiation at 1486.6 eV, with pass energy of 17.90 eV giving a resolution of 0.60 eV for the Ag ($3d_{5/2}$) standard. Data were processed using Casa XPS software. The same full width half maxima (fwhm) and Lorentzian-Gaussian curves were used to resolve the individual peaks for each element. Spectra were recorded using a take-off angle of 70° with respect to the sample surfaces. An electron flood gun was employed to neutralize charge build-up on the nonconductive films examined in this work. The electron flood gun was operated at 220 ma and 1.8 eV, conditions that provided optimum resolution of the C(1s) multiplet peaks. The C(1s) binding energies were established by centering the lowest binding energy peak of the C(1s) multiplets, corresponding to carbon atoms bonded only to other carbon or hydrogen atoms, at 284.6 eV (14a). The binding energies of the C 1s and O 1s multiplet peaks are in accord with literature values (14a) as are the values observed for the Ba and Ti atoms (14b).

X ray diffraction (XRD) data were collected at room temperature using a Bruker-AXS D8 Discover diffractometer equipped with a normal-focus Co tube (35 kV, 40 mA, Co Kα = 1.7902

Table 1. Pulsed Plasma Polymerization Conditions Employed for $BaTiO_3$ Nanoparticle Coating Using Ethylene Diamine Monomer

monomer used in plasma	on/off pulsed cycle (ms)	time (min)	peak power (W)	pressure (mtorr)	average power input[a] (W)
O_2	10/30	30	200	180	50
EDA	1/6	30	200	80	28.57
	1/10	30			18.18
	1/20	30			9.52
	1/30	30			6.45

[a] Average Power Input = (Power on time/total pulsed cycle time) × peak power.

Angstoms). Scans were collected between 30 and 80° 2θ, with a step-size of 0.1 and exposure time of 10 s per data point.

Infrared spectra were recorded on a vector 22 Fourier Transformed Infrared spectrometer from Bruker optics operated at a resolution of 8 cm^{-1}.

Transmission electron microscopy (TEM) images of the nanoparticles and nanocomposites were obtained using a FEI Tecnai G2 F20 S-Twin instrument operated at 120 kV. A drop of ethanol containing dispersed nanoparticles was placed on formvar coated copper grids, and the ethanol was allowed to evaporate at room temperature.

Scanning electron microscopy (SEM) images were recorded using a Zeiss Supra 55 VP instrument. All samples were coated with silver prior to analysis in order to avoid or minimize static charging effects.

Thermogravimetric analysis (TGA) was carried out on a Hi-Res TGA 2950 Thermogravimetric Analyzer from TA Instruments using platinum pan with a heating rate 10°C/ min under a continuous flow of nitrogen (up to 500 °C).

Diffential scanning calorimetry (DSC) was performed with a Diamond DSC from Perkin Elmer using aluminum pan at a scanning rate 40 °C/min under nitrogen (flow rate 20mL/min). Initially, all samples were thermally conditioned (up to 150 °C) to remove any thermal stress. A heating rate of 10°C/min, under nitrogen, was employed for this purpose. The glass transition temperatures (T_g) were determined by the standard half Cp extrapolated method from the second heating run, as obtained using Pyris software (Perkin Elmer).

The tensile properties of the samples were measured using an MTS Insight 2 instrument fitted with a 2000 N load cell and pneumatic grip (20 psi) and processed with MTS Test Works V 4.10A software. A cross-head speed of 2 mm/min was used at room temperature. Samples (dimensions 50 mm × 10 mm × ~0.5 mm, with free length of 10 mm.) were elongated to failure and the initial modulus was calculated by measuring the gradient at 0.75% of elongation of the stress-strain curve. A minimum of four specimens per sample were tested and averaged.

Plasma Treatment to Functionalize the BTO Particles. The PECVD treatment of the BTO nanoparticles was carried out using a custom built 360° rotating plasma reactor, capable of continuous operation under vacuum, as described elsewhere (15). The rotating, cylindrical glass reactor contained grooves on the inside walls to transport the particles upward for subsequent gravitational descent through the plasma discharge. The pulsed plasma cycles, peak RF power input, rotational speed of reactor (30 rpm) and duration of plasma discharge were optimized to create films which exhibited excellent long term stability to exposure to organic solvents (e.g. methanol, acetone, etc.). Prior to plasma polymerization, the BTO particles were subjected to a pretreatment in an oxygen plasma to remove any carbonaceous contaminants. Subsequently, the RF (13.56 MHz frequency) pulsed plasma was initiated at room temperature using ethylenediamine (EDA) as monomer. Initially, the plasma discharge was operated briefly at high input power to graft a carbonaceous-like layer to the BTO particles. The function of this layer is to help transition the inherent chemical incompatibility between the inorganic and organic components. At this initial high power density, essentially none of the nitrogen atoms in the EDA are retained in the deposited film. Subsequently, the average RF power input was slowly decreased by reduction of the plasma duty cycle, creating a gradient layered structure in which the amine content of the plasma deposited film increases as the pulsed plasma duty cycle was decreased (15c, 16). Although the ethylenediamine based macromolecular layer deposited on the BTO particles contains both primary and secondary amines, it is important to note that both of these amine groups react readily with the epoxide groups provided by the diglycidyl ether bisphenol organic matrix. The plasma parameters employed in the particle surface modification are summarized in Table 1.

Synthesis of Nanocomposites. Nanocomposites, containing either unmodified (**1**) or plasma functionalized (**2**) BTO particles, were synthesized using the bisphenol F diglycidyl ether resin (**3**). Additionally, pure solid epoxy polymer controls were prepared, without BTO particles, using the same synthesis route employed for the composites. Scheme 1 summarizes the general approach and synthetic conditions employed. Initially, the epoxy monomer was combined with specific amounts of modified or unmodified nanoparticles to create a series of samples having BTO weight content of 1, 2, 3, and 5 g per 100 g of the epoxy. The reactions were carried out at 60 °C, to reduce the viscosity of the epoxy monomer, using high speed stirring to maximize mixing efficiency. Degassing was performed by applying vacuum several times to remove entrapped air or moisture in the system. After mixing was completed, triethylene tetramine (TETA) was added to the reaction mixture to ensure complete curing of the epoxy. This mixture was further degassed and cured in to an open Teflon mold, having dimensions of 50 mm × 10 mm × 0.5 mm at room temperature for an initial 24 h, followed by a two hour exposure at 121 °C. Finally, the samples underwent a slow cooling process down to room temperature to assure complete curing of the samples.

Simplified sample identification employed to identify the various samples is as follows: **4** for pure polymer; **5** for the untreated BTO/polymer compositesl and **6** for the plasma treated BTO/polymer. Additional designations, such as **5.1**, **6.1**, ..., **5.5**, **6.5** are employed to identify the extent of nanoparticle loading of the respective composite materials, which consisted of samples containing 1.0−5.0 parts per hundred parts by weight (phr) of the epoxy matrix nanoparticle loading, as noted above (see Table 3).

RESULTS

XPS Analysis. The BTO nanoparticles, both unmodified (**1**) and modified (**2**), were analyzed by XPS. Both survey and high-resolution spectra are depicted in Figure 1. It should be noted that for (**1**), in addition to Ba, Ti, and O, carbon is also observed. Presumably, this carbon simply represents adsorbed organic compounds. Although this carbon is signifi-

Scheme 1. Reaction Sequence Illustrating the Formation of Epoxy−BTO Composites Having the Inorganic Particles Covalently Bonded to the Organic Matix

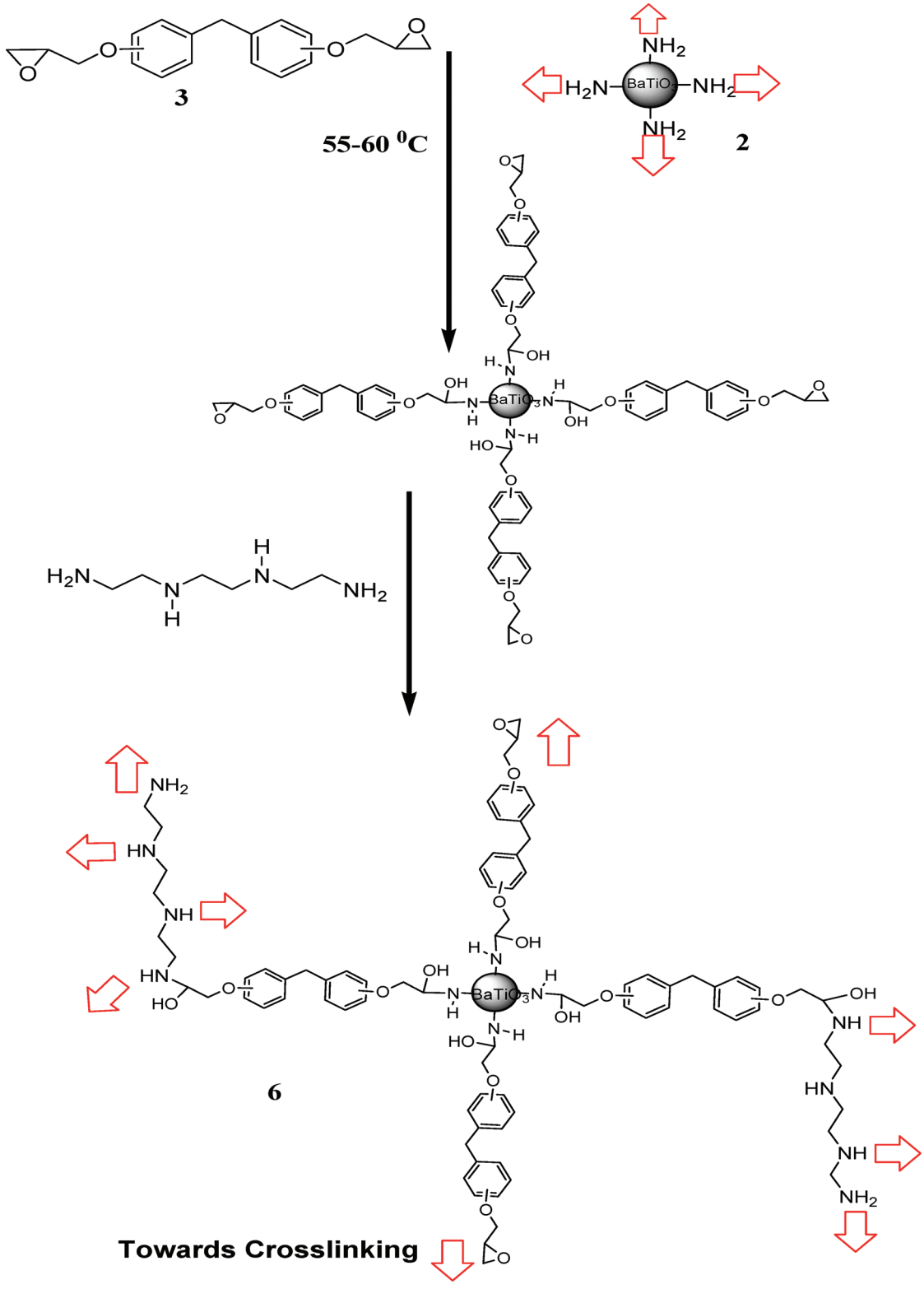

cantly reduced by a pretreatment of O_2 plasma, as reported previously. The XPS of the unmodified BTO was made on samples as-received (9c, 14b). The binding energies of O-1s, N-1s, C-1s, Ba-3d, and Ti-2p photoelectrons and surface compositions of both treated and untreated BTO particles, obtained from integration of the deconvoluted spectra, are summarized in Table 2. Both XPS survey and high resolution scans (Figure 1) illustrate that after plasma exposure of the BTO to the EDA, the relative atomic concentration of C-1s increases significantly. This is attributed to plasma deposition of C−C, C−N, and C═N surface functionalities on the particles. However, the presence of small amounts of oxi-

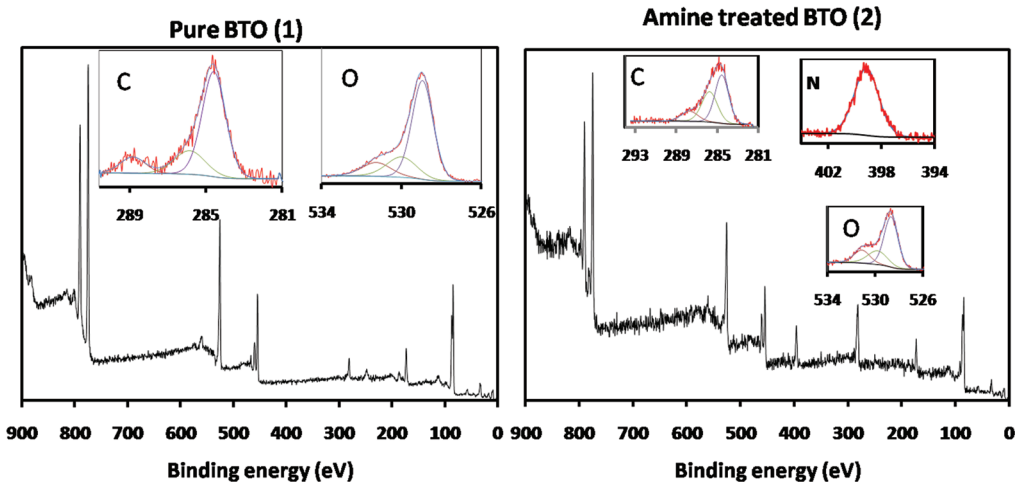

FIGURE 1. Survey and high-resolution XPS spectra of unmodified BTO (1) (left) and plasma modified BTO (2) (right) nanoparticles.

Table 2. Binding energies, possible surface species composition (%), and atomic concentration (%) of the BTO XPS spectra

	pure BTO (1)				amine-treated BTO (2)			
	binding energy (eV)	surface species composition (%)		atomic conc. (%)	binding energy (eV)	surface species composition (%)		atomic conc. (%)
O 1s	531.3	O−H	13.0	54.4	531.1	O−H	17.6	31.0
	530.0	bulk O^{2-}	19.5		529.8	bulk O^{2-}	22.6	
	528.9	C−O	67.5		528.6	C−O	59.8	
N 1s					399.6	C−N	12.12	12.1
C 1s	288.4	C═O	11.4	14.2	287.7	C═N,C≡N, C═O	12.9	41.2
	286.1	C−O−C C−O−H	20.6		285.8	C−NH_2 C−O−C, C−O−H	36.2	
	284.6	C−C	68.0		284.6	C−C	50.9	
Ti 2p	457.8	$2p_{3/2}$		14.8	457.9	$2p_{3/2}$		7.8
Ba 3d	778.0	$3d_{5/2}$		16.8	777.9	$3d_{5/2}$		7.9

dized carbon is also noted because of post plasma surface oxidation after plasma treatment. The increase of C1s concentration on the plasma treated particles surface is accompanied by a significant reduction in the atomic concentrations of Ba-3d, Ti-2p, and O-1s in comparing the treated and untreated BTO particles (Table 2). Most significant is the presence of N-1s (12.1%) photoelectrons on the plasma modified BTO. In contrast, no N atom photoelectrons are observed from the untreated BTO. Additionally, there is a significant difference in the structure of the C (1s) high-resolution spectra in comparing the treated and untreated BTO, which is consistent with conversion of the BTO surfaces from C−O contaminants to C−N chemistry (Figure 1 insets). The XPS samples were done in triplicate and the atom percent variations among the three samples were less than 2%. Because the differences in the atom percent compositions between untreated and treated particles are far greater than this 2% variation, the XPS data are interpreted to provide strong confirmation of surface modification of the BTO nanoparticles as a result of the plasma treatment.

Infrared Analysis. FT-IR spectroscopy provides additional evidence of the successful coating of the BTO particles. The IR spectra of the unmodified (**1**) and modified (**2**) BTO particles are shown in Figure 2. Several important distinctions are apparent. The IR spectrum (inset) of **1** shows (OH) stretching bands in the region between 3700 and 3200 cm^{-1}. The bands observed at 3680, 3640, 3583, 3510 cm^{-1} (sharp) and at 3424 cm^{-1} (broad) are attributed to OH groups on different sites and from interactions among them on the untreated BTO particles (17). The plasma treated BTO exhibits a reduction in absorption in the OH region, accompanied by a slight shift in peak maxima to lower wave numbers. These observations are consistent with the deposition of surface amine groups. Additionally, C−H stretching vibrations, around 2931 and 2870 cm^{-1} are present on this sample, but not on untreated BTO, consistent with the plasma deposition of the macromolecular layer obtained

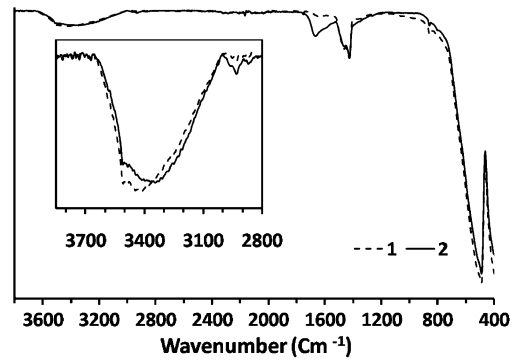

FIGURE 2. FTIR spectra of unmodified BTO (1) and plasma modified BTO (2).

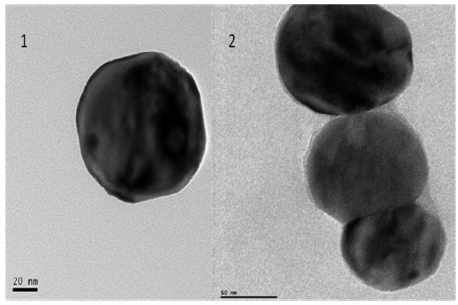

FIGURE 3. TEM images of unmodified BTO (1) and plasma-modified BTO (2) particles. Scale bar 20 and 50 nm, respectively.

from the EDA. Additional strong confirmatory evidence for the surface changes introduced by the plasma treatment is the appearance of the absorption band at 1665 cm^{-1}, which is consistent with the presence of a N−H deformation vibration.

FT-IR spectra of the starting monomer and the composites (not shown) clearly revealed the disappearance of the characteristic epoxide absorption bands at ∼1240 and ∼825 cm^{-1} of the monomer with formation of the pure polymer or the composites. Additionally, the polymer samples exhibited strong absorptions in the 3300−3400 cm^{-1} region from the presence of the NH groups. However, in agreement with the chemistry shown in Scheme 1, the IR spectra cannot reveal any absorption differences in contrasting the pure polymer and the composites in that the same basic coupling reactions are involved with or without modified BTO particles. As a result, these spectra were not included in this paper.

Microstructural Analyses. The spectroscopic results documenting the presence of the thin films on the plasma treated samples were further confirmed by TEM analyses of the unmodified and modified BTO particles. As shown in Figure 3, a thin film coating is discernable on the coated particles. Given the limitations of the TEM employed, it is not possible to ascribe a specific thickness to the plasma deposited films. The continued presence of photoelectrons from Ba and Ti atoms, as shown by the XPS data on the treated samples, indicates that the film thickness was, on average, less than the X-ray penetration depth of approximately ∼10 nm for the 70° take-off angles employed.

It was not possible to generalize about the extent of particle aggregation for the coated and uncoated dry particles from the TEM micrographs in that it varied for both types of particles from spot to spot. The pictures shown in Figure 3 simple illustrate the presence and absence of the plasma deposited film. However, as noted below, distinct differences were observed in the extent of particle aggregation in contrasting the untreated and treated composite materials.

Additional microscopic analyses included SEM studies of the unmodified and plasma modified particles as they appear in the final synthesized BTO-epoxy nanocomposites. The results obtained are shown in Figure 4, with the composite containing the plasma modified particles shown at a 2-fold higher resolution. Despite this higher resolution, it is

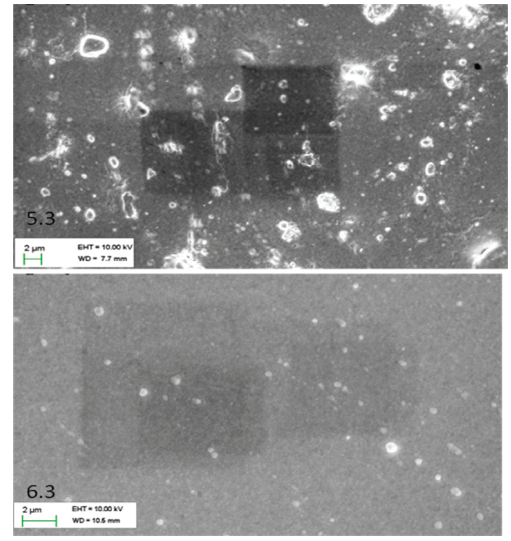

FIGURE 4. SEM picture comparing particle sizes and distributions in the synthesized 3 phr nanoparticle loaded BTO/ epoxy nanocomposites (top, untreated nanoparticles (5.3), scale bar = 2 μm, magnification = 2000×; bottom, plasma-modified nanoparticles (6.3), scale bar = 2 μm, magnification = 4240×).

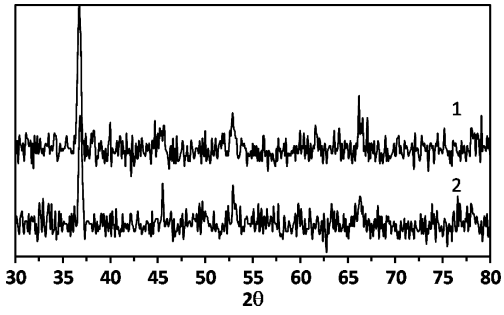

FIGURE 5. X-ray diffraction traces of unmodified (1, top) and plasma-modified (2, bottom) BTO nanoparticles.

clear than the modified particle sizes are significantly smaller, on average, and more uniformly dispersed than the unmodified particles. This is an important point in that the smaller average size for the treated particles suggests a significant decrease in the average extent of particle aggregation during synthesis of the composites, presumably as a result of the organic-based surface coatings and their more energetically favorable interactions with the organic matrix solution, compared to that achieved with the highly polar untreated BTO particles. As shown in Figure 3, the plasma treatment itself does not decrease the BTO particle size.

XRD Analysis. X-ray diffraction (XRD) studies were carried out to examine if the plasma treatment had affected the BTO crystal structure. Both untreated (**1**) and plasma treated (**2**) BTO samples were examined, as shown in Figure 5. As depicted, the major characteristic peaks (36.8, 45.6, 52.9, 63.3°) at 2θ values of BTO (18) are observed for both **1** and **2**. As these two traces reveal, the pulsed plasma discharge had no significant effect on the crystallinity of the BTO nanoparticles.

Mechanical Properties. The stress/strain properties of the pure polymer (**4**) and composites containing unmodified (**5**) and plasma modified (**6**) BTO particles were measured and contrasted. For the composites, BTO loadings of

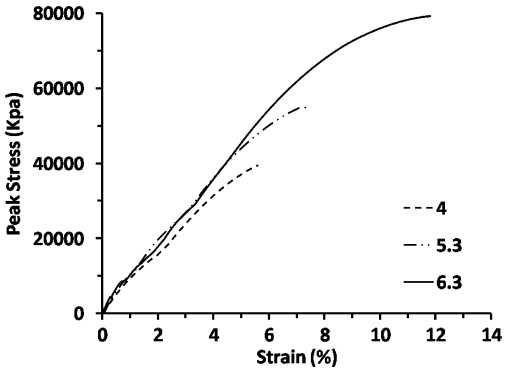

FIGURE 6. Stress-strain curves for pure epoxy polymer (4) and 3 phr nanoparticle loaded composites with untreated (5.3) and plasma-modified (6.3) BTO particles.

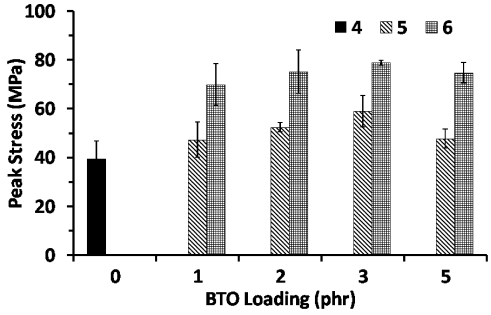

FIGURE 7. Peak stress at break for the pure epoxy polymer (4) and each of the composites containing unmodified (5) and plasma-modified (6) BTO particles.

1, 2, 3, and 5 parts per hundred were employed for each set of samples, as indicated by the designations **5.1**, **6.1**, etc. Figure 6 shows typical stress-strain curves for the pure epoxy polymer, as well as for samples containing unmodified and plasma modified BTO, in this case, for the 3 parts per hundred loaded samples (**5.3** and **6.3**, respectively). A nonlinear response was obtained for all three samples up to the break point, as commonly observed for polymeric materials. More importantly, we note the distinctly different break points for each sample, with the composites exhibiting greater elongation before breaking than the pure polymer. In particular, this elongation is significantly higher for the covalently bonded BTO sample (**6.3**) compared to the physically mixed (**5.3**) sample. Similar differences were observed in contrasting the samples having other percent loading. Figure 7 provides a compilation of the stress at break for other samples employed in this study. The percent elongations, at break, including the standard deviations, are shown in Figure 8.

The key physical properties, summarized in Table 3, include the modulus for each sample, as computed using the initial slopes from the stress-strain curves, including the standard deviations observed.

Thermal Properties. ***DSC Analysis.*** Significant differences in glass-transition temperatures (T_g) were observed in contrasting the DSC results of the pure polymer and composite materials, as shown in Figure 9. Both classes of composites reveal higher T_g values for the composites than for the pure epoxy polymer. Additionally, the T_g values for the composites containing the plasma modified BTO

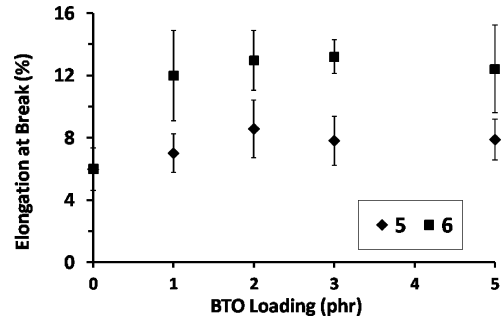

FIGURE 8. Percent elongation at break for the pure polymer (ordinate) and the composite samples (5, 6) as a function of nanoparticle loading (phr), as identified in the graph.

particles are uniformly higher than those for the physically mixed samples, at all loading levels. Percentage wise, the largest relative increase in T_g values are obtained for the 1 part per hundred loading, with subsequent smaller increases obtained for the 2 and 3 phr loaded samples. However, decreases in T_g were observed for both samples **5.5** and **6.5** when the loading is increased to 5 phr.

Representative comparison of DSC thermograms (Figure 10) for **4**, **5.3**, and **6.3** show that not only thermal properties but also microstructure of the resulting nanocomposites are strongly dependent on type of nanoparticles used (**1** or **2**). A broad thermal phase transition ranging from 60−120° C could be observed for composites containing unmodified BTO, suggesting nonuniform distributions and thus formation of discrete micro domains within the nanocomposites. In contrast, a relatively sharp phase change could be observed for composites containing the modified BTO, similar to pure resin **4**, indicating a more uniform distribution of particles within the matrix.

TGA Analysis. Thermal properties of all materials were also examined by means of thermogravimetric analysis, in runs carried out under N_2. Representative TGA curves for the pure epoxy polymer and the composites, containing 3 parts per hundred loading of unmodified and surface modified BTO, are shown in Figure 11. Also included in this figure are the thermograms for the unmodified (**1**) and plasma modified (**2**) BTO particles, illustrating the thermal stability of these particles. It is interesting to note that the very small weight loss for the plasma modified BTO sample, covering a relatively wide temperature range, is consistent with the presence of the gradient layered plasma deposited polyamine coating which has a sequential decrease in cross-link density extending outward from the particle surfaces. The TGA data for all polymer and composite samples are given in Table 4 in terms of the 5% weight loss temperatures (T_5) and weight percent residual char at 500° C. Clearly, the composites containing the surface modified particles (**6**) exhibit improved thermal stability relative to the pure polymer (**4**) and the composite containing the unmodified BTO particles (**5**). In fact, with respect to the initial 5% weight loss, the composites containing unmodified BTO exhibit slightly decreased thermal stability relative to the pure polymers.

In general, the TGA traces show a similar two-stage weight loss pattern for pure epoxy (**4**) as well as the nano-

Table 3. Summation of the Mechanical Properties of Pure Polymer (4) and the Nanocomposites Containing Unmodified (5) and Plasma-Modified (6) BTO particles, Having Loadings Ranging from 1 to 5 Parts BTO per 100 Parts Epoxy (phr)

sample	1 (phr)	2 (phr)	peak stress[a] (Mpa)	elongation at break[a] (%)	modulus ± SD[b] (MPa)
			Pure Epoxy Polymer		
4			39.36	6.0	1032 ± 21
			Unmodified BTO Nanocomposites		
5.1	1		47.18	7.0	1211 ± 119
5.2	2		52.26	8.6	1139 ± 80
5.3	3		58.87	7.8	1263 ± 122
5.5	5		47.68	7.9	1212 ± 99
			Plasma-Modified BTO Nanocomposites		
6.1		1	69.85	12	1229 ± 41
6.2		2	75.1	13	1223 ± 119
6.3		3	78.74	13.2	1295 ± 61
6.5		5	74.65	12.4	1225 ± 163

[a] Average values are given for the stress and elongation at break. [b] SD = standard deviation.

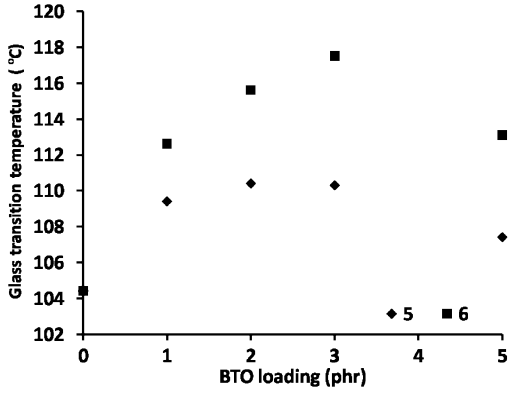

FIGURE 9. Glass-transition temperature (T_g) of pure epoxy polymer (ordinate) and nanocomposites containing unmodified (5) and amine surface-modified BTO particles (6).

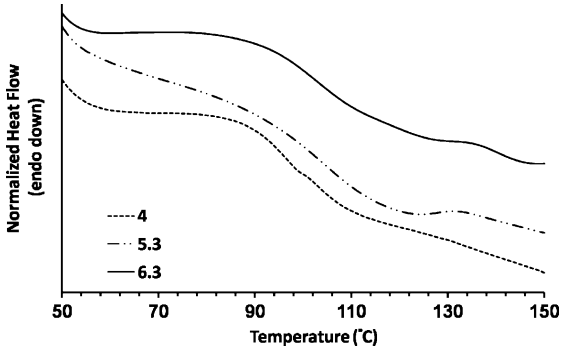

FIGURE 10. Representative DSC traces for pure polymer (4) and nanocomposites with unmodifed (5.3) and modified BTO (6.3).

composites (**5** or **6**). The differences in the thermal properties of these materials are more clearly distinguished in terms of the differential TGA (DTGA) data shown in Figure 12. The first large scale weight loss, starting at about ~335−360° C, is attributed to the loss of low-molecular-weight cyclic or linear organic components and is considered as the onset of decomposition of the polymer chain. The second weight loss, starting at around ~400−425 °C, is most likely decomposition of highly cross linked structures

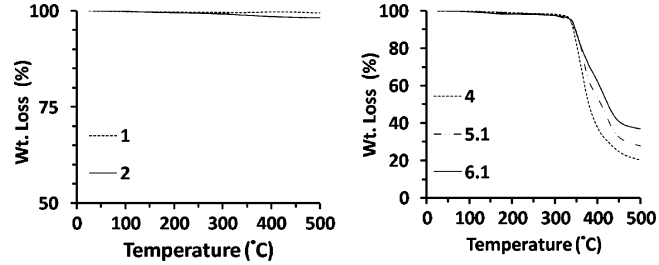

FIGURE 11. TGA traces for unmodified (1) and modified (2) BTO particles (left), and pure polymer (4) and nanocomposites with unmodified (5.1) and modified BTO (6.1) (right).

and hence strongly dependent on extent of nanoparticles loading, as well as type of nanocomposites (i.e., **5** or **6**). As shown in Figure 12, samples containing the BTO particles exhibit a decreased weight loss at the 335−360° C intervals, with this decrease being significantly larger for the composite containing the plasma modified BTO particles. The significantly improved thermal stability of the composites containing the plasma modified BTO particles is attributed to the reduced chain mobility in **6** (compared to **4** or **5**) because of covalent attachment of polymer chains to the nanoparticles. This increased cross-linking contributes to retarding radical chain transfer reactions, decreased escape of organic volatiles and reduced oxygen diffusion at higher temperature (19). In particular, this figure clearly reveals the enhanced thermal stability of the composite containing the covalently coupled BTO particles, relative to the physically mixed composite, with respect to shifting significant amounts of weight loss from the low-temperature to higher-temperature regime.

DISCUSSION

The primary objective of this work was to examine the efficacy of employing plasma surface modifications to improve the physical properties of inorganic/organic nanocomposites. As detailed above, we believe these objectives have been realized. As shown by the spectroscopic and micro-

Table 4. TGA Data of Pure Epoxy (4) and Nanocomposites with Unmodified (5) and Modified (6) BTO Particles

	sample no.								
	4	5.1	5.2	5.3	5.5	6.1	6.2	6.3	6.5
T_5[a] (°C)	336	330	331	334	326.5	340	342	339	343
residual char (wt %) at 500 °C	20.2	27.9	22.6	27	32.4	37	30.3	31.5	35.2

[a] T5: 5% weight loss temperature.

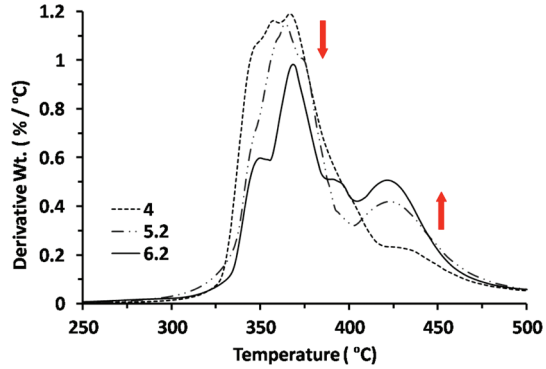

FIGURE 12. Representative DTGA traces for pure polymer 4 and its nanocomposites of unmodified (5.2) and modified BTO (6.2).

scopic results, the nanoparticle surface functionalizations were successfully achieved. The properties of the composites with the functionalized particles were indeed enhanced as shown by studies of both the mechanical and thermal characteristics of these materials. Importantly, these enhancements are achieved at relatively low loading levels, as expressed with respect to weight percent. Given the much higher density of the BTO relative to the epoxy, the loading factors for the fillers would be significantly less when expressed in terms of volume percents of filler compared to matrix. However, as others have noted, in dealing with nanoparticles, thin interfacial layers can actually represent significantly larger volumes when these interfacial contributions are included in the filler volumes (5e). Thus, it is possible to observe significant changes in composite properties even at relatively low weight percents of filler. This is particularly true in the present case in that the plasma treated particles appear significantly less aggregated in the composites compared to the composites formed with untreated particles. This decreased aggregation promotes enhanced interfacial interactions between particle and organic matrix.

The selection of depositing amine functionalities on the BTO particles was based on the known rapid reactions of these groups with epoxides, thus providing an opportunity to covalently couple the inorganic and organic components, in that way creating a novel class of more structurally integrated nanoparticle inorganic−organic composites. Mechanical properties of any composite system are highly dependent on effective load transfer ability from polymer matrix to reinforced filler. Obviously, the role of interfaces in composites is very important as it directs the load transfer capability or deformation from the matrix to the filler particles. This is particularly true with nanoparticles, given their high surface to volume ratios, thus tending to maximize the magnitude of interfaces between polymer and inorganic fillers. In light of the results obtained in the present study, it appears that this load transfer capability can be significantly enhanced by covalently bonding these nanoparticles to the polymer matrix, as opposed to the simple physical mixing of the inorganic and organic components.

With respect to measurement of the physical properties, elongation-to-break indicates the rupture behavior of composite materials and generally decreases with increased filler loading (12j, 20). However, unusual results were observed for elongation at break in this study. Elongation at break follows the same trend as tensile strength, increasing as the percent loading was varied from 1 to 3 g of BTO per 100 g of epoxy resin. The maximal value of 13.2% elongation for the samples containing the modified BTO is significantly higher than the 8.6% observed for the unmodified particles or the 6% elongation for pure epoxy polymer. The results suggest that the nano fillers may improve both the failure behavior and energy absorption of nanocomposites by acting as crack growth stoppers, without interrupting polymer matrix deformation significantly (20c). Nevertheless, there is clearly a limit to the useful extent of loading in that the elongation-to-break properties decreased at 5 g to 100 g loading level. This result suggests that perhaps rigidity of the inorganic particles have begun to impart increased brittleness in the composites.

With respect to thermal properties, the improved stabilities of the composites at higher temperatures, relative to the pure polymer, is attributed to restrictions in chain mobility of the matrix resulting from filler−matrix interaction. Furthermore, it is also clear that T_g values of the composites containing the modified particles are consistently higher than those materials containing the unmodified BTO. It is well-known that for a given thermosetting polymeric system, cross-link density is one of the important factors that affect T_g values (12j). For nanocomposites, mobility of nanoparticles is an important factor, which is a function of nanoparticle dimension, the matrix−nanoparticle interaction, and the thermodynamic state of the matrix (12j, 21). In the present case, direct chemical attachment of nanoparticles with the matrix act as a cross-linking point, which further reduces the molecular motion of polymer chains, thus contributing to an increased T_g. This restricted segmental movement not only increases the T_g but also improves the overall thermal stability of the nanocomposites, as evidenced by the TGA results (Figures 11 and 12). It is interesting to note that, in common with the mechanical properties, a reduction of T_g above 3 parts per hundred loading is observed for both types of composites. It is not clear why the reduction in T_g values is observed. Planned additional studies, such as examination of these properties with a range

of nanoparticles of different size and having different surface densities of reactive functional groups, will hopefully shed light on this important topic.

We conclude by noting that the basic approach described in this work is one of general utility in that it can be applied to virtually any nanoparticle and, dependent on monomer choice employed in the plasma step, can be used to introduce a wide range of functionalities on the particles. As such, it provides an unusual opportunity to explore the properties of nanocomposites having a broad spectrum of inorganic and organic materials. We are currently involved in examining this possibility, including extension of these studies to include elastomers.

CONCLUSION

The plasma polymerization approach provides a convenient all-gas phase technique to introduce reactive organic functional groups unto the surfaces of inorganic nanoparticles. The adhesion of the polymer films on the particles is sufficiently strong to permit synthesis of inorganic/organic composites having improved particle dispersions and thus significantly improved physical properties, achieved at relatively low loading of the inorganic components.

Acknowledgment. The authors thank CART- University of North Texas for use of their TEM imaging facilities and Paul Ubrich from Hexion Speciality Chemicals (Texas) for a generous donation of epoxy resins and amine. We also appreciate the assistance provided by Professor Jian Yang of the UTA Bioengineering Department with the measurements of the mechanical properties of the materials synthesized.

REFERENCES AND NOTES

(1) (a) Kickelbick, G. *Prog. Polym. Sci.* **2003**, *28*, 83, and references therein. (b) Balazs, A. C.; Emrick, T.; Russell, T. P. *Science* **2006**, *314* (17), 1107, and references therein. (c) Chowdhury, S. R.; Kar, S.; Ha, C.-S. Polymer nanocomposites: a promising class of materials for a wide range of applications. In *Polymeric Nanostructures and Their Applications*; Nalwa, H. S., Ed.; American Scientific: Valencia, CA, 2007; Vol. 2, pp 201−242. (d) Alexandre, M.; Dubois, P. Nanocomposites. In *Macromolecular Engineering*; Matyjaszewski, K., Gnanou, Y., Leibler, L., Eds.; Wiley−VCH: Weinheim, Germany, 2007; Vol. 4, pp 2033−2070. (e) Crosby, A. J.; Lee, J.-Y. *Polym. Rev.* **2007**, *47*, 217, and references therein. (f) Krishnamoorti, R.; Vaia, R. A. *J. Polym. Sc., Part B: Polym. Phys.* **2007**, *45*, 3252, and references therein. (g) Pavlidoua, S.; Papaspyrides, C. D. *Prog. Polym. Sci* **2008**, *33*, 1119, and references therein. (h) Rozenberg, B. A.; Tenne, R. *Prog. Polym. Sci* **2008**, *33*, 40, and references therein. (i) Kumara, A. P.; Depana, D.; Tomerb, N. S.; Singh, R. P. *Prog. Polym. Sci* **2009**, *34*, 479, and references therein. (j) Lue, C.; Yang, B. J. *Mater. Chem.* **2009**, *19*, 2884.

(2) (a) Vaia, R. A.; Giannelis, E. P. *Macromolecules* **1997**, *30*, 7990. (b) Ray, S. S.; Okamoto, M. *Prog. Polym. Sci.* **2003**, *28*, 1539, and references therein. (c) Alexandre, M.; Dubois, P. *Mater. Sci. Eng., R* **2000**, *28*, 1.

(3) (a) Kwiatkowski, K. C.; Lukehart, C. M. In *Handbook of Nanostructured Materials and Nanotechnology*; Nalwa, H. S., Ed.; Academic Press: New York, 2000; Vol. 1, pp 387−421. (b) Kuan, H.-C.; Chiu, S.-L.; Chen, C.-H.; Kuan, C-F.; Chiang, C.-L. *J. Appl. Polym. Sci.* **2009**, *113* (3), 1959. (c) Mark, J. E. *Heterog. Chem. Rev.* **1996**, *3*, 307. (d) Wu, C.-H. *J. Polym. Sci., Part A: Polym. Chem.* **2005**, *43*, 1690.

(4) (a) Gersappe, D. *Phys. Rev. Lett.* **2002**, *89* (5), 058301. (b) Graff, R. A.; Swanson, J. P.; Barone, P. W.; Baik, S.; Heller, D. A.; Strano, M. S. *Adv. Mater.* **2005**, *17*, 980. (c) Lee, J.-Y.; Zhang, Q.; Emrick, T.; Crosby, A. J. *Macromolecules* **2006**, *39*, 7392. (d) Ciprari, D.; Jacob, K.; Tannenbaum, R. *Macromolecules* **2006**, *39*, 6565. (e) Lee, J.-Y.; Su, K. E.; Chan, E. P.; Zhang, Q.; Emrick, T.; Crosby, A. J. *Macromolecules* **2007**, *40*, 7755. (f) Tong, Y. J.; Li, Y. S.; Xie, F. C.; Ding, M. X. *Polym. Int.* **2000**, *49*, 1543. (g) Liu, L.; Lu, Q. H.; Yin, J.; Qian, X. F.; Wang, W. K.; Zhu, Z. K. *Mater. Chem. Phys.* **2002**, *74*, 210. (h) Chiang, P. C.; Whang, W. T. *Polymer* **2003**, *44*, 2249.

(5) (a) Kovacevic, V.; Lucic, S.; Leskovac, M. *J. Adhes. Sci. Technol.* **2002**, *16*, 1343. (b) Kovacevic, V.; Leskovac, M.; Lucic, B. S. *J. Adhes. Sci. Technol.* **2002**, *16*, 1915. (c) Petrovic, Z. S.; Javni, I.; Wasson, A.; Banhegyi, G. *J. Appl. Polym. Sci.* **2000**, *76*, 133. (d) Tannenbaum, R.; Zubris, M.; David, K.; Cipari, D.; Jacob, K.; Jasiuk, I.; Dan, N. *J. Phys. Chem. B* **2006**, *110*, 2227. (e) Wu, C. L.; Zhang, M. Q.; Rong, M. Z.; Friedrick, K. *Comput. Sci. Technol.* **2002**, *62*, 1327.

(6) (a) Rong, Y.; Chen, H.-Z.; Wu, G.; Wang, M. *Mater. Chem. Phys.* **2005**, *91*, 370. (b) Bourgeat-Lami, E.; Lang, J. *J. Colloid Interface Sci.* **1998**, *197*, 293.

(7) (a) Marcinko, S.; Fadeev, A. Y. *Langmuir* **2004**, *20*, 2270. (b) Fadeev, A. Y.; McCarthy, T. J. *Langmuir* **2000**, *16*, 7268. (c) Helmy, R.; Wenslow, R. W.; Fadeev, A. Y. *J. Am. Chem. Soc.* **2004**, *126*, 7595.

(8) (a) Gamble, L.; Jung, L. S.; Campbell, C. T. *Langmuir* **1995**, *11*, 4505. (b) Kim, H.; Colavita, P. E.; Paoprasert, P.; Gopalan, P.; Kuech, T. F.; Hamers, R. J. *Surf. Sci.* **2008**, *602*, 2382.

(9) (a) Leu, C.-M.; Wu, Z.-W.; Wei, K.-H. *Chem. Mater.* **2002**, *14*, 3016. (b) Lin, Y.; Zhou, B.; Fernando, K. A. S.; Liu, P.; Allard, L. F.; Sun, Y.-P. *Macromolecules* **2003**, *36*, 7199. (c) Zhu, J.; Peng, H.; Rodriguez-Macias, F.; Margrave, J. L.; Khabashesku, V. N.; Imam, A. M.; Lozano, K.; Barrera, E. V. *Adv. Funct. Mater.* **2004**, *14*, 643. (d) Hill, D.; Lin, Y.; Qu, L.; Kitaygorodskiy, A.; Connel, J. W.; Allard, L. F.; Sun, Y.-P. *Macromolecules* **2005**, *38*, 7670. (e) Qu, L.; Veca, L. M.; Lin, Y.; Kitaygorodskiy, A.; Chen, B.; McCall, A. M.; Connel, J. W.; Sun, Y. P. *Macromolecules* **2005**, *38*, 10328. (f) Zhou, Q.; Wang, S.; Fan, X.; Advincula, R. *Langmuir* **2002**, *18*, 3324. (g) Fan, X.; Xia, C.; Advincula, R. C. *Langmuir* **2005**, *21*, 2537.

(10) (a) Vollath, D.; Szab'o, D. V. *J. Nanopart. Res.* **1999**, *1*, 235. (b) Shi, D. L.; Wang, S. X.; Ooij, W. J.; Wang, L. M.; Zhao, J. G.; Yu, Z. *Appl. Phys.Lett.* **2001**, *78*, 1243. (c) Weinkauf, D. H.; Harper-Nixon, D.; Wyatt, J.; Jeon, H. S. *Abstr. Am. Chem. Soc.* **2002**, *224*, IEC-049. (d) Shi, D.; He, P. *Rev. Adv. Mater. Sci.* **2004**, *7*, 97. (e) Nastase, C.; Nastase, F.; Vaseashta, A.; Stamatin, I. *Prog. Solid State Chem.* **2006**, *34*, 181. (f) Guo, Y.; Cho, H.; Shi, D.; Lian, J.; Song, Y.; Abot, J.; Poudel, B.; Ren, Z.; Wang, L.; Ewing, R. C. *Appl. Phys. Lett.* **2007**, *91*, 261903. (g) Ramos-deValle, L. F.; Neira-Vela'zquez, M. G.; Herna'ndez-Herna'ndez, E. *J. Appl. Polym. Sci.* **2008**, *107*, 1893. (h) Chou, J.-W.; Wang, C.-C.; Chen, C.-Y. *Polym. Degrad. Stab.* **2008**, *93*, 745. (i) Wang, Y.; Zhang, J. *J. Macromol. Sci., Part B: Phys.* **2006**, *45*, 899. (j) Zhu, F.; Kong, E. S.-W.; Zhang, J.; Zhang, Y. *Chem. Phys. Lett.* **2006**, *423*, 270. (k) Sawada, Y.; Kogoma, M. *Powder Technol.* **1997**, *90*, 245.

(11) Oeoye, G.; Roucoules, V.; Oates, L. J.; Cameron, A. M.; Cameron, N. R.; Steel, P. G.; Badyal, J. P. S.; Davis, B. G.; Coe, D. M.; Cox, R. A. *J. Phys. Chem. B* **2003**, *107*, 3496.

(12) (a) Zhu, J.; Kim, J. D.; Peng, H.; Margrave, J. L.; Khabashesku, V. N.; Barrera, E. V. *Nano Lett.* **2003**, *3*, 1107. (b) Hsueh, H.-B.; Chen, C.-Y. *Polymer* **2003**, *44*, 5275. (c) Qi, L.; Lee, B. I.; Chen, S.; Samuels, W. D.; Exarhos, G. J. *Adv. Mater.* **2005**, *17*, 1777. (d) Cho, S.-D.; Jang, K.-W.; Hyun, J.-G.; Lee, S.; Paik, K.-W.; Kim, H.; Kim, J.-H. *IEEE Trans. Electron. Packag. Manuf.* **2005**, *28*, 297. (e) Qi, L.; Lee, B. I.; Samuels, W. D.; Exarhos, G. J.; Parler, S. G. *J. Appl. Polym. Sci.* **2006**, *102*, 967. (f) Ramajo, L. A.; Reboredo, M. M.; Castro, M. S. *J. Mater. Sci.* **2007**, *42*, 3685. (g) Ramajo, L.; Castro, M. S.; Reboredo, M. M. *Composites, Part A* **2007**, *38A*, 1852. (h) Dang, Z.-M.; Yu, Y.-F.; Xu, H.-P.; Bai, J. *Compos. Sci. Technol.* **2008**, *68*, 171. (i) Chiu, Y.-C.; Liu, F.-Y.; Ma, C.-C. M.; Chou, I.-C.; Riang, L.; Chiang, C.-L.; Yang, J.-C. *Thermochim. Acta* **2008**, *473*, 7. (j) Chatterjee, A.; Islam, M. S. *Mater. Sci. Eng., A* **2008**, *A487*, 574. (k) Chau, J. L. H.; Tung, C.-T.; Lin, Y.-M.; Li, A.-K. *Mater. Lett.* **2008**, *62*, 3416.

(13) (a) Kim, P.; Jones, S. C.; Hotchkiss, P. J.; Haddock, J. N.; Kippelen, B.; Marder, S. R.; Perry, J. W. *Adv. Mater.* **2007**, *19*, 1001. (b) Popielarz, R.; Chiang, C. K.; Nozaki, R.; Obrzut, J. *Macromolecules* **2001**, *34*, 5910.

(14) (a) Wagner, C. D.; Riggs, W. M.; Davis, L. E.; Moulder, J. F.; Mullenberg, G. E. *Handbook of X-Ray Photoelectron Spectroscopy*; Perkin-Elmer Corp.: Eden Prairie, MN, 1979. (b) Ehre, D.; Cohen,

H.; Lyahovitskaya, V.; Lubomirsky, I. *Phys. Rev. B: Condens. Matter* **2008**, *77*, 184106/1.
(15) (a) Thevenot, P.; Cho, J.; Wavhal, D.; Timmons, R. B.; Tang, L. *Nanomed.: Nanotechnol., Biol. Med.* **2008**, *4*, 226, and references therein. (b) Martin, A. R.; Manolache, S.; Denes, F. S.; Mattoso, L. H. C. *J. Appl. Polym. Sci.* **2002**, *85*, 2145. (c) Cho, J.; Denes, F. S.; Timmons, R. B. *Chem. Mater.* **2006**, *18*, 2989.
(16) (a) Timmons, R. B.; Griggs, A. J. Pulsed plasma polymerizations. In *Plasma Polymer Films*; Biedermann, H., Ed.; World Scientific: Hackensack, NJ, 2004; pp 217−245 and references therein. (b) Mukherjee, N.; Wavhal, D.; Timmons, R. B. *Polym. Prepr. (Am. Chem. Soc., Div. Polym. Chem.)* **2009**, *50* (1), 385.
(17) (a) Busca, G.; Buscaglia, V.; Leoni, M.; Nanni, P. *Chem. Mater.* **1994**, *6*, 955. (b) Chang, S.-J.; Liao, W.-S.; Ciou, C.-J.; Lee, J.-T.; Li, C.-C. *J. Colloid Interface Sci.* **2009**, *329*, 300. (c) Noma, T.; Wada, S.; Yano, M.; Suzuki, T. *J. Appl. Phys.* **1996**, *80*, 5223.
(18) Su, K.; Nuraje, N.; Yang, N.-L. *Langmuir* **2007**, *23*, 11369.
(19) (a) Modesti, M.; Lorenzetti, A.; Besco, S.; Hrelja, D.; Semenzato, S.; Bertani, R.; Michelin, R. A. *Polym. Degrad. Stab.* **2008**, *93*, 2166. (b) Chen, J.; Zhou, Y.; Nan, Q.; Sun, Y.; Ye, X.; Wang, Z. *Appl. Surf. Sci.* **2007**, *253*, 9154. (c) Khaled, S. M.; Sui, R.; Charpentier, P. A.; Rizkalla, A. S. *Langmuir* **2007**, *23*, 3988.
(20) (a) Zhang, M.; Zeng, H.; Zhang, L.; Lin, L.; Lin, G.; Li, R. K. Y. *Polym. Compos.* **1993**, *1*, 357. (b) Wu, C. L.; Zhang, M. Q.; Rong, M. Z.; Friedrick, K. *Comput. Sci. Technol.* **2002**, *62*, 1327. (c) Roulin-Moloney, A. C. *Fractography and Failure Mechanisms of Polymer and Composites*; Elsevier Applied Science: London, 1986.
(21) (a) Rangari, V. K.; Koltypin, Y. U.; Gedanken, A. *J. Appl. Polym. Sci.* **2002**, *86*, 160. (b) Wu, C. L.; Zhang, M. Q.; Rong, M. Z.; Friedrick, K. *Comput. Sci. Technol.* **2005**, *65*, 635. (c) Nicolais, L.; Narkis, M. *Polym. Eng. Sci.* **1971**, *11*, 194. (d) Chisholm, N.; Mahfuz, H.; Rangari, V. K.; Ashfaq, A.; Jeelani, S. *Comput. Struct.* **2005**, *67*, 115. (e) Miyagawa, H.; Drzal, L. T. *Polymer* **2004**, *45*, 5163.

AM900677S